Ultramicroscopy 153 (2015) 32–39

Contents lists available at ScienceDirect

Ultramicroscopy

journal homepage: www.elsevier.com/locate/ultramic

Combining structural and chemical information at the nanometer scale by correlative transmission electron microscopy and atom probe tomography

M. Herbig *, P. Choi, D. Raabe

Max-Planck-Institut für Eisenforschung, Department of Microstructure Physics and Alloy Design, 40237 Düsseldorf, Germany

ARTICLE INFO

Article history:
Received 21 June 2014
Received in revised form
5 February 2015
Accepted 12 February 2015
Available online 14 February 2015

Keywords:
Correlative microscopy
APT
TEM
Nanobeam diffraction
Orientation mapping
ASTAR
HRTEM

ABSTRACT

In many cases, the three-dimensional reconstructions from atom probe tomography (APT) are not sufficiently accurate to resolve crystallographic features such as lattice planes, shear bands, stacking faults, dislocations or grain boundaries. Hence, correlative crystallographic characterization is required in addition to APT at the exact same location of the specimen. Also, for the site-specific preparation of APT tips containing regions of interest (e.g. grain boundaries) correlative electron microscopy is often inevitable. Here we present a versatile experimental setup that enables performing correlative focused ion beam milling, transmission electron microscopy (TEM), and APT under optimized characterization conditions. The setup was designed for high throughput, robustness and practicability. We demonstrate that atom probe tips can be characterized by TEM in the same way as a standard TEM sample. In particular, the use of scanning nanobeam diffraction provides valuable complementary crystallographic information when being performed on atom probe tips. This technique enables the measurement of orientation and phase maps as known from electron backscattering diffraction with a spatial resolution down to one nanometer.

1. Introduction

For answering many materials science-related questions, correlative chemical and crystallographic knowledge at the nanometer (nm) scale is required. Examples are numerous and include local phase transformations triggered by segregation [31]; the investigation of precipitation [15] and partitioning phenomena [35]; the characterization of the formation of oxide layers [5] and radiation-induced microstructural changes [26]; the prove that there is no segregation at a lattice defect above the detection limit of APT [25]; the investigation of correlations between segregation and dislocations [6], stacking faults [7], or for understanding the correlation between solute segregation and the character of grain boundaries [14,20,36,4,8]. Atom probe tomography (APT), having the capacity to measure three-dimensional (3D) chemistry with equal detection sensitivity (of a few ppm) for all elements at near atomic spatial resolution [16], can provide answers to some of these questions. In certain cases, the spatial resolution of APT is even high enough to preserve three or more independent lattice planes in the 3D atom maps, enabling unambiguous indexing of grain orientations [1,23,28,39,40]. However, the spatial resolution is material- and measurement condition-dependent. For instance, the spatial resolution usually improves with lower measurement temperature and fewer alloying elements. The ideal material for crystallographic APT analyses has large lattice spacing and shows a regular field evaporation behavior such that the atomic planes are field evaporated in a defined sequence from outside to inside, layer by layer. This behavior is disturbed by lattice defects and by the presence of high concentrations or local enrichments of elements that have a different field evaporation potential than the matrix element. Hence, in most cases, sufficient crystallographic information required for a full-picture description of certain phenomena remains inaccessible by APT alone.

Transmission electron microscopy (TEM), on the other hand, is an excellent tool for structural investigation, even down to sub-Ångstrom scale. However, analytical TEM is often less suited than APT for the quantification of 3D local chemical compositions at the atomic scale. Firstly, TEM suffers from projection effects that make the investigation of non-planar features challenging, and secondly, in the case of chemical analysis by energy-dispersive X-ray spectroscopy and electron energy loss spectroscopy in the TEM, the quantification of absolute concentration values is difficult due to complex spectra that often require deconvolution of integrated signals obtained from illuminated atomic columns, and signals

* Corresponding author.
E-mail address: m.herbig@mpie.de (M. Herbig).

http://dx.doi.org/10.1016/j.ultramic.2015.02.003
0304-3991/

that are dependent on many optical parameters [9,17,38]. This holds true especially for low concentrations of light elements embedded in a heavy element matrix. APT has the advantage that the atoms, field-evaporated as ions, are simply identified by their mass-to-charge ratio through time-of-flight spectroscopy, which renders the analysis of absolute concentration values comparatively robust.

The complementary nature of TEM and APT (see also [34]) suggests that both techniques should be subsequently applied to the same sample in order to combine their strengths. This was already realized and subsequently put into practice by Fasth, Loberg and Nordén in the 1960s [10,24], who investigated the sample shape by single-tilt TEM, before and after field-ion microscopy experiments. After the introduction of TEM for the target preparation of grain boundaries in the apex of FIM samples by Papazian [29], Kraukauer and Seidman [18] developed a setup in the 1990s that enabled double-tilt TEM operation followed by one-dimensional atom probe measurements on individual atom probe (AP) tips. More recent and sophisticated approaches have allowed for TEM tomography on individual AP tips prior to APT [13,2], for the purpose of optimization of the reconstruction parameters. In recent years, experimental setups capable of holding several atom probe tips at once have been developed, drastically increasing specimen throughput [11,12]. Following on from these, we present here a versatile experimental setup based on a modified, commercial, high-angle single-tilt TEM retainer, which enables correlative focused ion beam (FIB), scanning electron microscopy (SEM), TEM and APT. Several crucial aspects have been improved compared to former approaches. The exact control of the sample orientation in all instruments makes precise merging of information measured in different devices possible, and enables measurement of atom probe tips in TEM under optimized characterization conditions. The grid containing the atom probe samples can now safely be inserted and extracted from the setup due to an improved grid-holding mechanism and due to a grid design that enhances sample protection. This makes the transfer of the samples to any other standard double-tilt TEM retainer a straightforward procedure, thereby enabling experiments under controlled diffraction conditions and high resolution TEM (HRTEM). Moreover, we introduce the usage of (scanning) nano-beam diffraction (NBD) on AP tips. With this powerful tool, local crystallographic analyses with a spatial resolution of 2 nm or better can be performed on AP tips and even the first 10 nm of AP tips prepared by FIB milling can be investigated.

2. Materials and methods

The method development was performed on two iron-based material systems: a binary Fe–9Mn (wt%) martensitic alloy, annealed for two days at 450 °C to create small austenitic, Mn-enriched precipitates; and a hypereutectoid pearlitic steel with composition Fe–0.98C–0.31Mn–0.20Si–0.20Cr (wt%), cold-drawn by $\varepsilon = 6.02$ true strain and annealed for 2 min at 400 °C to create a microstructure composed of columnar grains with an average diameter of about 30 nm and some intergranular cementite particles [22].

The samples were extracted from the surface of the bulk material by standard FIB lift-out procedures, deposited on a bisected, electropolished TEM grid, and subsequently measured by TEM and then APT as described by Felfer et al. [11]. The approach described here pays special attention to gain exact control of the sample orientation in all instruments in order to optimize characterization conditions in each instrument, to create damage tolerance during sample manipulation, allow transfer of samples into other standard TEM holders, and to simplify electropolishing. The detailed experimental setup and procedure is given below.

A commercial molybdenum TEM grid (1GM 100, Pyser-SGI) was fixed between two glass slides and cut using a razor blade, two grid rows above the center (Fig. 1a). This procedure effectively avoids bending of the grid which is a prerequisite to guarantee that all samples are within the range of the eucentric height in TEM. It is also important for protection of the electropolished tips and the samples during grid manipulation. Only if the tips are located right on the center plane of an undistorted grid point, can it be guaranteed that the grid can be laid with both sides onto a flat substrate without damage to the tips. The larger half of the bisected grid was then mounted at its outermost end into a v-shaped holder specifically designed for electropolishing (Fig. 1b). Using a v-shaped adapter for electropolishing (Fig. 1b) has the

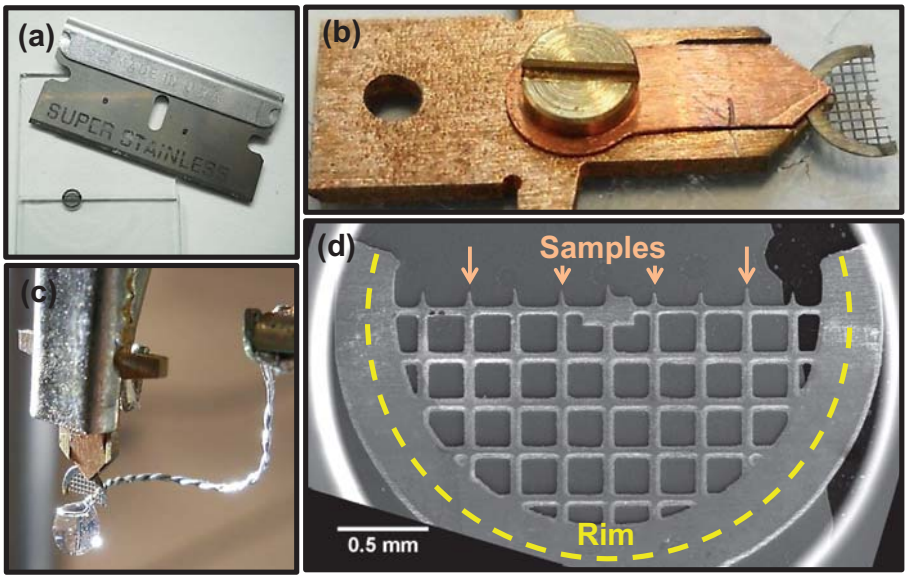

Fig. 1. Preparation of a commercial TEM grid for sample deposition by a FIB lift-out procedure. (a) Sectioning of grid fixed between two glass slides using a razor blade. (b) Mounting of grid into special holder for electropolishing. (c) Setup during electropolishing. (d) SEM micrograph of electropolished grid. Only the posts of the grid are shortened and tapered during electropolishing, ready for FIB lift-out sample deposition. The rim of the grid is not removed and serves as protection for the samples against mechanical damage.

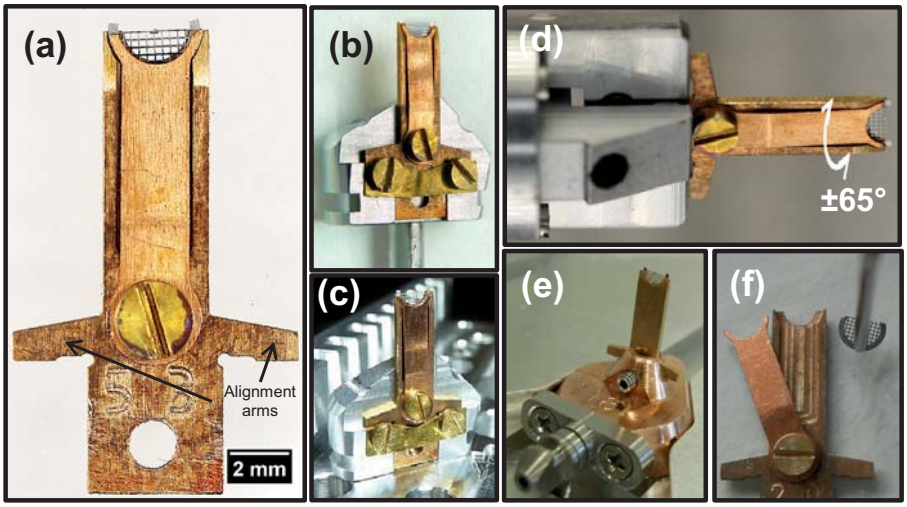

Fig. 2. The "grid holder" (a modified JEOL EM-21311HTR high-angle single-tilt TEM retainer) is the core part of the experimental setup. The use of adapters assures compatibility in all instruments and provides exact control of the sample orientation. (a) The grid holding section is tapered to avoid blocking the incident or exiting electron beam by any parts of the holder in the TEM. The two arms at the side serve as a mechanical limit stop for the alignment in all instruments. (b) The adapter employed during FIB milling. (c) Experimental setup during FIB sample preparation. (d) The grid holder fits directly into a JEOL TEM single-tilt holder. (e) Modification of a Cameca puck specimen assembly that allows the insertion of the grid holder into the local electrode atom probe (LEAP) instrument. (f) Insertion/extraction of the grid using a vacuum 'tweezer' holding tool.

advantage that the grid is held at a single pivot point, which allows for fine adjustment of the tip heights during electropolishing by dipping the grid on one side deeper into the electrolyte than on the other. As such, the tips can be brought to an even height, which is important to avoid field-evaporation of adjacent tips during the APT measurements. The inner posts were tapered/sharpened by electropolishing in an aqueous solution of 10% NaOH using ~5 V DC, down to a tip length of about 100 μm above the center row, and to a final tip diameter of around two microns (Fig. 1c, d). The outer rim of the grid is kept longer than the tips for sample protection during grid manipulation. Detailed information on this preparation procedure is also available as a video [8].

The core part of the experimental setup consists of a modified replica of a JEOL EM-21311HTR high-angle single-tilt TEM retainer (termed "grid holder" here, for reasons of simplicity) for a JEOL JEM-2200FS microscope. In the version used for this study, the front/end half of the grid-holding section has been removed and the front ends are tapered (Fig. 2a). The electropolished grid is placed into the grid holder using a vacuum tweezer (Fig. 2f). Rotational misalignment between posts of the grid and the grid holder was minimized using the cross-hair of a stereo microscope. A long working distance objective lens of 15 mm allows for manual operation with a small screw driver directly under the stereo microscope. The compatibility of the grid holder to all instruments was achieved by the use of custom-designed adapters shown in Fig. 3b, c and e.

For FIB milling the grid holder was inserted into an adapter which was aligned vertically into the universal mounting base (Fig. 2c) in a FEI Helios Nanolab 600i dual-beam FIB instrument. By a standard lift-out procedure [11] four samples were deposited on electropolished grid posts. During annular milling of the samples the stage was tilted to 52° so that the grid holder's tilt axis was parallel to the ion beam. For single-tilt TEM measurements the grid holder was directly inserted into a JEOL JEM-2200FS microscope operating at 200 kV. The clamping mechanism of the grid holder makes the transfer of the samples to any other standard TEM retainer using a vacuum holding tool, a straight-forward procedure (Fig. 2f). This enables measurement of AP tips in virtually all TEMs. For double-tilt measurements described here the grid was transferred into a double-tilt TEM retainer and then back into the grid holder to conduct the APT measurements. APT was performed in a Local Electrode Atom Probe 3000X HR (LEAP™,

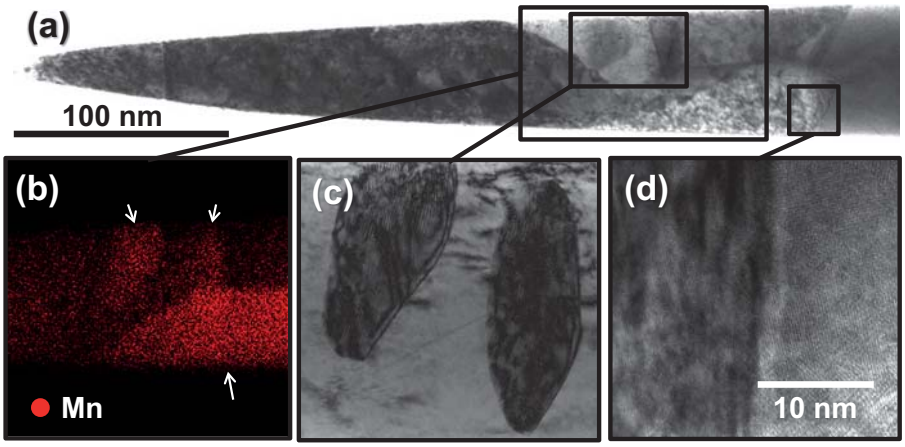

Fig. 3. TEM analysis performed on an AP tip. (a) BF-STEM micrograph of a martensitic Fe–9Mn alloy containing Mn-enriched precipitates. (b) STEM-EDX analysis of the Mn distribution showing two small and one large austenitic Mn-enriched precipitates (white arrows). (c) BF-TEM magnification of two austenitic precipitates containing stacking faults. (d) HRTEM image of an austenite (left)/martensite (right) interface.

Cameca Instruments). A well-defined slit was spark-eroded into a commercial puck specimen assembly, to create compatibility between grid holder and the instrument (Fig. 2e). Samples were measured in the order of the length of their post, starting with the longest.

3. Results and discussion

3.1. Transmission electron microscopy

The experimental setup allows for a single-tilt TEM range of about $\pm 65°$ for the inner tips and $\pm 50°$ for the outermost tips. Fig. 3a shows a bright-field (BF) scanning TEM (STEM) image of an atom probe tip from the tempered martensite Fe–9Mn alloy. For this investigation the grid was transferred into a double-tilt TEM retainer to enable the selection of well-defined orientation relations between grains and the incident beam, thereby enabling diffraction experiments and HRTEM imaging along specific crystallographic zone axes. The sample was subjected to FIB milling at 5 kV in the final step of preparation. Due to its slim shape the sample did not exceed 60 nm thickness within the first 400 nm along the tip axis. Thus, good imaging quality could be achieved at 200 kV in this region. Fig. 3b shows a STEM-EDX micrograph of the Mn distribution. The local enrichments of Mn indicate that the sample contains one large and two small austenite precipitates. BF-TEM (Fig. 3c) under controlled diffraction conditions reveals that the left precipitate contains several stacking faults. Fig. 3d shows a high resolution TEM image taken from the interface region between martensitic matrix and the austenitic precipitate.

Since the spatial resolution of selected area diffraction (SAD) is limited by the diameter of the smallest aperture available ($\sim$50 nm), the nanobeam diffraction (NBD) technique (also referred to as small angle convergent beam electron diffraction) must be performed in order to obtain diffraction patterns from individual grains with smaller diameter. The spatial resolution of the NBD orientation mapping is limited by the combination of several effects, namely, the spot size of the focused electron beam, the convergence angle and the sample thickness [42], it can reach values down to 1 nm [27,32]. For indexing of the NBD patterns, alignment of a certain zone axis with respect to the incident beam is not required. Grain orientations can be measured with an angular resolution $\leq 1°$ and individual phases can also be identified [33].

Fig. 4a shows a BF-STEM micrograph of a pearlitic atom probe tip that received final FIB milling at 2 kV. The columnar grains are oriented in beam direction. Fig. 4b shows the NBD pattern measured at the topmost part of the sample on a grain with a lateral size of 10 nm $\times$ 13 nm and $\sim$10 nm thickness. This diffraction pattern was collected in STEM spot mode (0.5 nm spot size) on a phosphor screen using a condenser lens aperture of 10 μm with 1 s exposure time, and its orientation (Fig. 4c) was determined using the commercial software TOCA [41]. This manual measurement

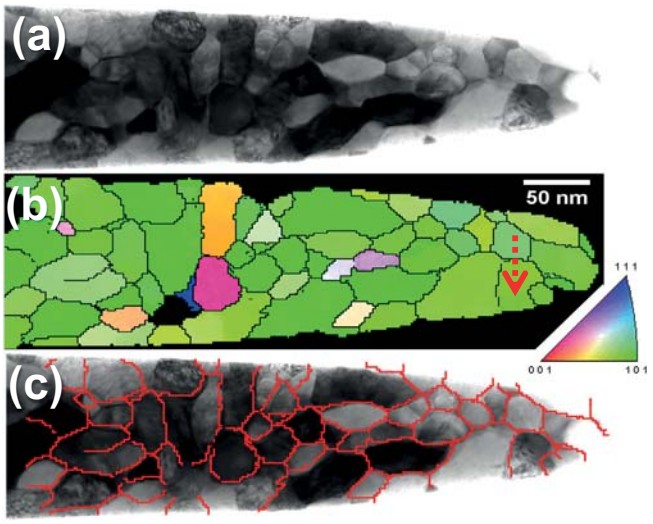

Fig. 5. (a) BF-STEM micrograph of an atom probe tip prepared from cold-drawn pearlite by FIB milling. The columnar grains are oriented parallel to the incident beam to minimize grain overlap. (b) Inverse pole figure map measured by NBD of ferrite. The grain boundary network (black lines) was automatically generated. The red arrow marks the grain boundary discussed in Fig. 6. (c) The overlay of this automatically generated grain boundary network with the BF-image shows excellent agreement. (For interpretation of the references to color in this figure legend, the reader is referred to the web version of this article.)

routine is suited for materials which contain only a few grains per atom probe sample (grain sizes $>$ 100 nm) and which exhibit only negligible intra-granular orientation gradients. Fig. 4 demonstrates that NBD can even be used on the very top of an AP tip prepared by FIB milling if the sample preparation is performed carefully enough. This region is directly exposed to the gallium beam, where beam damage is most likely to occur.

For materials with grain sizes below 100 nm or with strong orientation gradients, NBD orientation mapping is better suited than the manual routine described above. Fig. 5 shows a second pearlitic atom probe tip in the same orientation, on which automated scanning nanobeam diffraction was conducted (nanobeam orientation mapping) using the commercial ASTAR setup (NanoMEGAS SPRL) [27,33]. The scan was performed in NBD mode, using a 10 μm condenser lens aperture, 0.5 nm spot size, 2 nm step size and 40 ms exposure time. This setup resulted in a total acquisition time of about 15 min. The indexed orientation map was exported to the commercial OIM^{TM} Data Analysis (EDAX Inc.) software to automatically generate a network of all grain boundaries with misorientation angles above 5° (Fig. 5b). The overlay of this grain boundary network with the STEM image shows excellent agreement (Fig. 5c). By using this technique, crystallographic orientation and phase maps, as per electron backscattered diffraction (EBSD) in SEM, can be acquired at the spatial resolution of NBD (Fig. 5b shows an NBD scan using 2 nm step size). Additionally, all

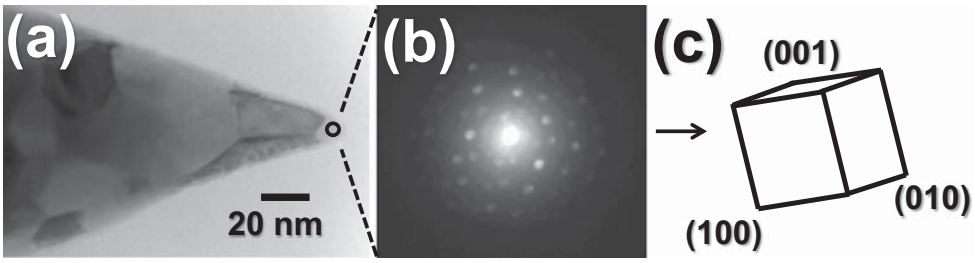

Fig. 4. (a) BF-STEM micrograph of an atom probe tip prepared from cold-drawn pearlite by FIB milling. (b) NBD pattern acquired at the topmost ferrite grain from (a). (c) Visualization of corresponding grain orientation after indexing with TOCA.

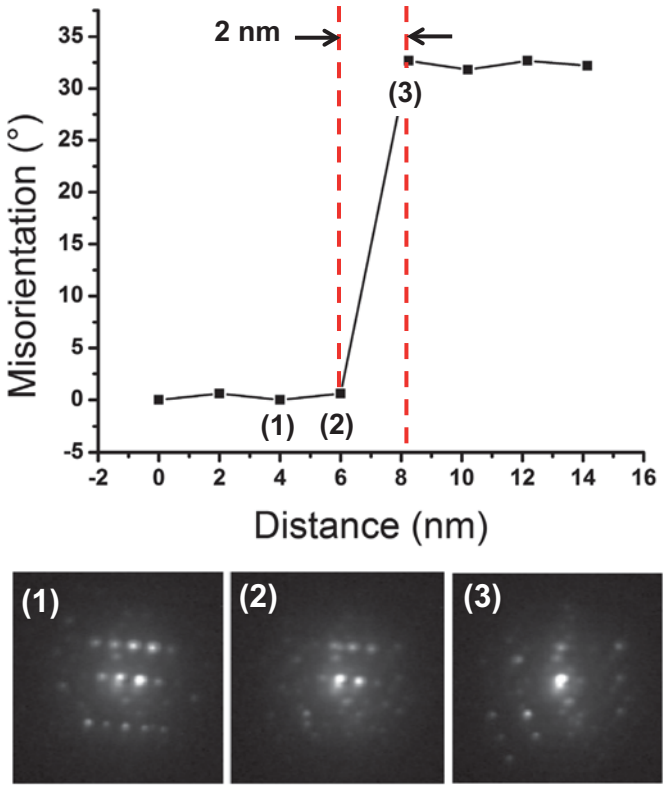

Fig. 6. Misorientation traverse across the grain boundary marked with a red arrow in Fig. 5b. Individual NBD diffraction patterns across the interface are shown from three pixels. These measurements are spaced 2 nm apart. Significant superposition of individual diffraction patterns is only observed for a single pixel (diffraction pattern 2) across the boundary. (For interpretation of the references to color in this figure legend, the reader is referred to the web version of this article.)

local NBD patterns are saved, enabling further detailed offline diffraction analysis. Bright-field and dark-field STEM images of the samples can be generated from the local diffraction dataset. The possibility to export the datasets into commercial EBSD analysis software allows application of all standard EBSD processing and analysis tools also on atom probe tips. Furthermore, NBD allows for identification of crystallographic phases, even on atom probe tips [35]. Babinsky et al. recently demonstrated that transmission Kikuchi diffraction (TKD) can be employed to investigate grain orientations directly on AP tips [3]. This SEM-based orientation mapping technique was also recently demonstrated to show improved spatial resolution as compared to EBSD; 6–8 nm in a Ni sample [37]. This can be assumed to also apply for Fe due to the comparable atomic mass of the two elements. Fig. 6 shows the point-to-origin misorientation plot across an interface from the NBD orientation map shown in Fig. 5b. An abrupt change of the grain orientation within 2 nm distance is visible, which indicates a lateral spatial resolution of 2 nm for this technique. This result is backed up by the detailed study of individual NBD patterns across the interface (bottom of Fig. 6). Significant superposition of individual diffraction patterns is only observed for a single pixel. It is possible that better values could have been achieved since this particular measurement was limited by an applied step size of 2 nm. Rauch et al. demonstrate that even a spatial resolution down to 1 nm can be achieved using this technique on conventional TEM samples [32]. NBD orientation mapping is a highly automated way to link measurement positions with orientation and phase information with a lateral spatial resolution that is at least a factor three improved as compared to TKD and thus is a powerful tool for correlative TEM/APT.

The experimental setup and approach described here allows for almost damage-free FIB preparation of samples that lie within the plane of the TEM grid and are available for transfer into any standard TEM retainer. Figs. 3–4 demonstrate that all standard TEM techniques, including STEM imaging, to EDX, NBD and HRTEM, can successfully be performed on AP tips just like on ordinary TEM lamellas or foils. This opens the door for a wide range of complementary characterization techniques on AP tips. One application for STEM-EDX would be the identification of sparse precipitates in the AP tips to conduct their target preparation (e.g. Mn-rich precipitates in Fig. 3b). An application for TEM imaging would be the measurement of stacking fault widths (Fig. 3c) prior to their local chemical investigation by APT. An application for HRTEM would be the measurement of local atomic relaxation at an interface, before determining the level of segregation by APT. The main difference between conventional TEM samples and AP tips is the sample geometry, where several advantages exist for the characterization of AP tips by TEM. The confined sample volume makes it easy to locate the same region after tilting the sample. The sample thickness can be easily calculated from the width of the conical AP tips. Also, due to the small sample volume, astigmatism correction is not required for ferromagnetic materials such as pearlite when moving the sample or changing the tilt-angle in TEM.

3.2. Atom probe tomography

APT characterization of the pearlitic samples was performed at 250 kHz and 70 K, in voltage mode, using 1% target detection rate, and 15% pulse fraction. Fig. 7 shows an overlay of the carbon distribution as measured by APT with a BF-STEM image of the same sample. The parameters for the reconstruction of the APT map were optimized using the STEM image as a template. Best agreement between STEM image and the 3D atom map was achieved by conducting a shank angle reconstruction using 30 nm tip radius and 7° half shank angle. However, the true sample outline is best described by ~50 nm tip radius and ~10° half shank angle, as quantified from the STEM micrograph. The difference in tip radius can be explained by the fact that the first atoms measured in the AP experiment were not considered for the reconstruction. The difference in shank angle is due to the limited field of view of APT. That there is a difference between true specimen outline and the APT reconstruction parameters that yield the optimum match also implies that sample outlines as measured in the SEM can only serve as a rough guideline for reconstruction and that TEM micrographs which provide additional information of the sample interior are better suited for the adjustment of the reconstruction parameters. The combined information of local grain orientations as measured by NBD, grain boundary planes as measured from the STEM micrographs and the local chemistry measured by APT, enables the investigation of grain boundary segregation and its dependence on the five macroscopic degrees of freedom of the interface, for materials with grain sizes as low as 30 nm. The method thus provides an efficient way to measure a large number of boundaries [14,30].

3.3. Alignment between experimental components

A crucial part of this characterization approach lies in the optimal alignment between the different instruments, the grid holder, the grid and the specimen tips. In the TEM, two degrees of freedom (DOFs) are fixed by a flat contact between the grid holder and TEM holder. The remaining third DOF is fixed by moving the two alignment arms of the grid holder up against the TEM holder (Fig. 2d). The same principle is applied between grid holder and the adapters used for FIB milling and APT, which in turn have a

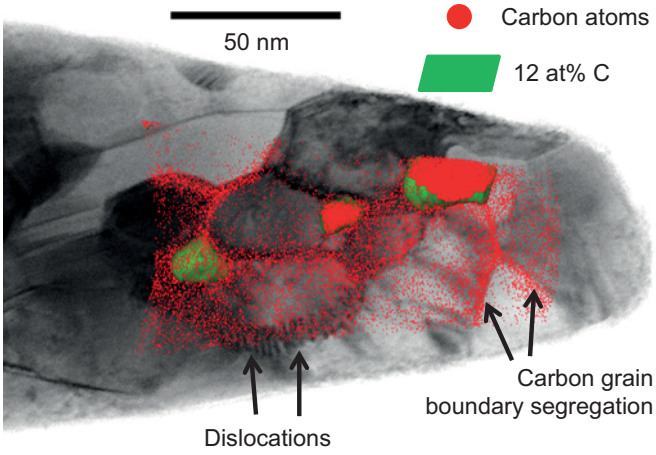

Fig. 7. Overlay of BF-STEM micrograph and projected 3D carbon map from APT. The STEM micrograph was used to optimize APT reconstruction parameters, yielding excellent agreement between STEM and APT. The 12 at% iso-concentration surface indicated in green indicates the position of the cementite particles. Individual dislocation lines are visible at low-angle grain boundaries. (For interpretation of the references to color in this figure legend, the reader is referred to the web version of this article.)

defined orientation relationship to their respective instrument. In the dual-beam FIB instrument, this alignment makes it possible to orient the length axis of the grid holder (which is the single-tilt axis in TEM) parallel to the incident ion beam. Atom probe tips prepared using this arrangement will be situated within the center plane of the grid. Apart from the difference in geometry from the typically flat TEM samples, the grid can be handled like any other 3 mm TEM sample. The characterization procedures required for the AP tips in TEM consequently do not differ from the ones applied on flat TEM samples. The AP tips can thus be handled and characterized in TEM just like any ordinary TEM lamellae or foils.

Sample preparation using the arrangement described above also means that the axes of rotational symmetry of all AP tips will be parallel to the single-tilt axis of the grid holder. By using the translational DOFs in TEM, the axis of rotational symmetry of one sample at a time can be brought into coincidence with the TEM single-tilt axis. The corresponding AP tip will then be in focus everywhere at the same time throughout the whole single-tilt range. This provides not only optimum characterization conditions but also simplifies the experiment as the sample hardly moves and only marginal focus changes must be done during the single-tilt experiment.

The geometrical arrangement of the samples in the different instruments is reproducible i.e. after extracting the samples from an instrument they can easily be mounted again in exactly the same orientation. This is especially important for the site-specific preparation of certain regions of interest (e.g. grain boundaries) for APT analyses. Such a scenario involves the iterative measurement of the position of the region of interest (ROI) by TEM and shortening of the tips by FIB milling until the ROI is located in the very apex of the APT tip. There is a risk of beam damage when re-inserting samples that are slightly inclined with respect to the ion beam. Due to the slim conical sample shape, sideward ion impact can easily cause beam damage down to the core of the sample. The reproducibility of the alignment in the FIB assures that there is no sideward beam impact when shortening the tips.

The reproducibility and exact control of the geometrical arrangement of the samples in the different instruments is also important for correctly merging the results and for linking TEM data to the 3D chemical information from APT. Examples where this is required include crystallographic TEM analysis of precipitates and interfaces or dislocations that are otherwise only visible in APT as chemical inhomogenities within the reconstructed dataset. A further necessity for correctly merging information from all different instruments is the careful measurement and compensation of the magnetic rotations between TEM images, NBD in STEM spot mode, and NBD orientation mapping.

For TEM experiments that require transfer of the grid into another TEM retainer and reinsertion into the grid holder the exact alignment between samples and grid holder is disrupted. For such cases the possible rotational misalignment of the grid before and after mounting the sample can be minimized by positioning the grid into the grid holder always at the same rotation angle with the help of the cross hair in a stereoscope.

3.4. Challenges arising from the correlative use of TEM and APT

The yield in an AP experiment (total number of ions collected before the sample fractures) is reduced after performing TEM investigations on the tip, which is mainly due to carbon contamination. Carbohydrate molecules are readily absorbed on the surface of the tips, grid and sample holder during exposure to air. In the presence of an electron beam (in the TEM or SEM) they accumulate to form caps on the AP tips. In order to field-evaporate this carbon cap during the AP experiment, a relatively high voltage needs to be applied due to the high field evaporation potential of carbon, and the high field can cause a burst of field evaporation that causes fracture. Alternatively, once the carbon cap is removed/evaporated, the field required to have done this is often relatively too high for the underlying specimen material, and this scenario can also cause a large burst of field evaporation of the specimen material and subsequently cause the sample to fracture. Another source of carbon contamination situated very close to the AP tip is the adhesive joint. In the current work, adhesion of the FIB lift-out specimen to the Mo grid post was facilitated using a Pt-based reactive gas, which is common among commercial FIB systems. Especially for high deposition rates, the Pt-bond contains high amounts of unreacted species (Pt precursor gas molecules), and upon exposure to the electron beam these molecules can be cracked and form carbon contamination layers. The authors have never observed a difference in the carbon content within samples measured by APT, when comparing samples that were measured in a FEG-TEM operated at 200 kV prior to the AP experiment, with samples that were measured by APT immediately after their FIB-based preparation. This indicates that no significant amount of carbon diffusion occurs from inside the sample to the tip surface during TEM characterization. Also, formation of oxide layers or the absorption of gaseous species causing embrittlement (e.g. hydrogen) during the time between sample preparation and APT, which is prolonged by performing a TEM experiment in between, can cause a reduction of the yield in the AP. Carbon contamination can be effectively avoided or even entirely removed by plasma cleaning using oxygen radicals. These react with the carbohydrates to form CO, CO_2 and H_2O, which are then removed by the vacuum pumps [21]. Williams and Carter [38] point out that plasma cleaning should be done prior to the TEM or SEM experiment but Krakauer and Seidman [19] demonstrate that these layers can also be successfully removed from APT tips after the TEM experiment. Oxide layers cannot be removed by plasma cleaning (because of its oxidative nature) and thus must be removed by sputtering, e.g. by further FIB milling. For reasons of efficiency, the material-specific AP measurement parameters that deliver best yield and data quality should be calibrated on dummy samples before performing correlative TEM experiments on AP tips.

4. Conclusions

We present a robust and versatile experimental setup and approach that enables easy-to-use correlative FIB/TEM and APT experiments with high throughput of samples. Exact control of sample orientation in all instruments allows for measurement under optimum acquisition conditions and for accurate merging of the output from different techniques. The setup is especially suited to perform high-angle single-tilt TEM experiments on AP tips but also allows transfer of the samples to any other standard TEM retainer. This opens the door to performing, in principle, all TEM techniques also on AP tips. As long as the FIB specimen preparation is performed carefully so as to avoid beam damage, and the sample is also thin enough, an AP tip can be characterized in TEM like any other conventional TEM sample with flat geometry. Under such conditions excellent NBD patterns can even be obtained from the topmost 10 nm of the AP tip. The conical shape of an AP tip also offers the advantage of ease of assessment of the local thickness. The time between sample preparation and AP measurement should be minimized and plasma cleaning can be performed to remove carbon contamination to increase the yield in the AP experiment. The approach described here was customized for the correlative use of a FEI Helios NanoLab 600i Dual-Beam FIB/SEM, a JEOL JEM-2200FS TEM and a LEAP 3000X HR atom probe but the principle should be applicable to almost any combination of microscopes.

Acknowledgements

The authors acknowledge financial support by the German Research Foundation that funded the project through SFB 761 “steel ab initio”, Aleksander Kostka and Stefan Zaefferer for the support with the TEM investigations, Ross Marceau for proofreading and the mechanical workshop of the MPIE for the construction of grid holders and adapters. The authors acknowledge Peter Felfer in particular for fruitful discussions and for sharing his expertize on the development of his approach for correlative TEM/APT [11].

References

[1] V.J. Araullo-Peters, B. Gault, S.L. Shrestha, L. Yao, M.P. Moody, S.P. Ringer, J. M. Cairney, Atom probe crystallography: atomic-scale 3-D orientation mapping, Scr. Mater. 66 (11) (2012) 907–910. http://dx.doi.org/10.1016/j.scriptamat.2012.02.022.

[2] I. Arslan, E.A. Marquis, M. Homer, M.A. Hekmaty, N.C. Bartelt, Towards better 3-D reconstructions by combining electron tomography and atom-probe tomography, Ultramicroscopy 108 (12) (2008) 1579–1585. http://dx.doi.org/10.1016/j.ultramic.2008.05.008.

[3] K. Babinsky, R. De Kloe, H. Clemens, S. Primig, A novel approach for site-specific atom probe specimen preparation by focused ion beam and transmission electron backscatter diffraction, Ultramicroscopy 144 (2014) 9–18. http://dx.doi.org/10.1016/j.ultramic.2014.04.003.

[4] S.I. Baik, M.J. Olszta, S.M. Bruemmer, D.N. Seidman, Grain-boundary structure and segregation behavior in a nickel-base stainless alloy, Scr. Mater. 66 (10) (2012) 809–812. http://dx.doi.org/10.1016/j.scriptamat.2012.02.014.

[5] S.I. Baik, X. Yin, D.N. Seidman, Correlative atom-probe tomography and transmission electron microscope study of a chemical transition in a spinel on an oxidized nickel-based superalloy, Scr. Mater. 68 (11) (2013) 909–912. http://dx.doi.org/10.1016/j.scriptamat.2013.02.025.

[6] D. Blavette, E. Cadel, A. Fraczkiewicz, A. Menand, Three-dimensional atomic-scale imaging of impurity segregation to line defects, Science 286 (5448) (1999) 2317–2319. http://dx.doi.org/10.1126/science.286.5448.2317.

[7] E. Cadel, A. Fraczkiewicz, D. Blavette, Suzuki effect on {001} stacking faults in boron-doped FeAl intermetallics, Scr. Mater. 51 (5) (2004) 437–441. http://dx.doi.org/10.1016/j.scriptamat.2004.04.026.

[8] O. Cojocaru-Miredin, T. Schwarz, P.P. Choi, M. Herbig, R. Wuerz, D. Raabe, Atom probe tomography studies on the Cu(In,ga)Se2 grain boundaries, J. Vis. Exp. (74) (2013), http://dx.doi.org/10.3791/50376.

[9] R.F. Egerton, Electron energy-loss spectroscopy in the TEM, Rep. Prog. Phys. *72* (1) (2009), http://dx.doi.org/10.1088/0034-4885/72/1/016502.

[10] J.E. Fasth, B. Loberg, H. Norden, Preparation of contamination-free tungsten specimens for field-ion microscope, J. Sci. Instrum. 44 (12) (1967) 1044. http://dx.doi.org/10.1088/0950-7671/44/12/428.

[11] P.J. Felfer, T. Alam, S.P. Ringer, J.M. Cairney, A reproducible method for damage-free site-specific preparation of atom probe tips from interfaces, Microsc. Res. Tech. 75 (4) (2012) 484–491. http://dx.doi.org/10.1002/Jemt.21081.

[12] B.P. Gorman, D.R. Diercks, N. Salmon, E. Stach, G. Amador, C. Hartfield, Hardware and techniques for cross-correlative TEM and atom probe analysis, Microsc. Today *16* (4) (2008) 42–47.

[13] D. Haley, T. Petersen, S.P. Ringer, G.D.W. Smith, Atom probe trajectory mapping using experimental tip shape measurements, J. Microsc. 244 (2) (2011) 170–180. http://dx.doi.org/10.1111/j.1365-2818.2011.03522.x.

[14] M. Herbig, D. Raabe, Y.J. Li, P. Choi, S. Zaefferer, S. Goto, Atomic-scale quantification of grain boundary segregation in nanocrystalline material, Phys. Rev. Lett. 112 (12) (2014), http://dx.doi.org/10.1103/Physrevlett.112.126103.

[15] T. Homma, M.P. Moody, D.W. Saxey, S.P. Ringer, Effect of Sn addition in pre-precipitation stage in Al–Cu alloys: a correlative transmission electron microscopy and atom probe tomography study., Metall. Mater. Trans. A – Phys. Metall. Mater. Sci. 43A (7) (2012) 2192–2202. http://dx.doi.org/10.1007/s11661-012-1111-y.

[16] T.F. Kelly, D.J. Larson, Atom probe tomography 2012, Annu. Rev. Mater. Res. 42 (2012) 1–31. http://dx.doi.org/10.1146/annurev-matsci-070511-155007.

[17] G. Kothleitner, M.J. Neish, N.R. Lugg, S.D. Findlay, W. Grogger, F. Hofer, L. J. Allen, Quantitative elemental mapping at atomic resolution using X-ray spectroscopy, Phys. Rev. Lett. 112 (8) (2014), http://dx.doi.org/10.1103/Physrevlett.112.085501.

[18] B.W. Krakauer, J.G. Hu, S.M. Kuo, R.L. Mallick, A. Seki, D.N. Seidman, R.J. Loyd, A system for systematically preparing atom-probe field-ion-microscope specimens for the study of internal interfaces, Rev. Sci. Instrum. 61 (11) (1990) 3390–3398. http://dx.doi.org/10.1063/1.1141590.

[19] B.W. Krakauer, D.N. Seidman, Systematic procedures for atom-probe field-ion microscopy studies of grain-boundary segregation, Rev. Sci. Instrum. 63 (9) (1992) 4071–4079. http://dx.doi.org/10.1063/1.1143214.

[20] B.W. Krakauer, D.N. Seidman, Subnanometer scale study of segregation at grain boundaries in an Fe(Si) alloy, Acta Mater. 46 (17) (1998) 6145–6161. http://dx.doi.org/10.1016/S1359-6454(98)00262-6.

[21] T. Levesque, Review of plasma cleaning technology for decontamination in FIB, SEM and TEM, Microsc. Anal. 25 (6) (2011) 11–14.

[22] Y.J. Li, P. Choi, S. Goto, C. Borchers, D. Raabe, R. Kirchheim, Evolution of strength and microstructure during annealing of heavily cold-drawn 6.3 GPa hypereutectoid pearlitic steel wire, Acta Mater. 60 (9) (2012) 4005–4016. http://dx.doi.org/10.1016/j.actamat.2012.03.006.

[23] P.V. Liddicoat, X.Z. Liao, Y.H. Zhao, Y.T. Zhu, M.Y. Murashkin, E.J. Lavernia, S. P. Ringer, Nanostructural hierarchy increases the strength of aluminium alloys, Nat. Commun. (2010), http://dx.doi.org/10.1038/Ncomms1062.

[24] B. Loberg, H. Norden, Observations of field-evaporation end form of tungsten, Ark. Fys. 39 (4) (1969) 383–395.

[25] R.K. Marceau, I. Gutierrez-Urrutia, M. Herbig, K.L. Moore, S. Lozano-Perez, D. Raabe, Multi-scale correlative microscopy investigation of both structure and chemistry of deformation twin bundles in Fe–Mn–C steel, Microsc. Microanal. (2013) 1–5. http://dx.doi.org/10.1017/S1431927613013494.

[26] E. Meslin, M. Lambrecht, M. Hernandez-Mayoral, F. Bergner, L. Malerba, P. Pareige, A. Almazouzi, Characterization of neutron-irradiated ferritic model alloys and a RPV steel from combined APT, SANS, TEM and PAS analyses, J. Nuclear Mater. 406 (1) (2010) 73–83. http://dx.doi.org/10.1016/j.jnucmat.2009.12.021.

[27] P. Moeck, S. Rouvimov, E.F. Rauch, M. Veron, H. Kirmse, I. Hausler, S. Nicolopoulos, High spatial resolution semi-automatic crystallite orientation and phase mapping of nanocrystals in transmission electron microscopes, Cryst. Res. Technol. 46 (6) (2011) 589–606. http://dx.doi.org/10.1002/crat.201000676.

[28] M.P. Moody, B. Gault, L.T. Stephenson, D. Haley, S.P. Ringer, Qualification of the tomographic reconstruction in atom probe by advanced spatial distribution map techniques, Ultramicroscopy 109 (7) (2009) 815–824. http://dx.doi.org/10.1016/j.ultramic.2009.03.016.

[29] J.M. Papazian, Preparation of field-ion-microscope specimens containing grain boundaries, J. Microsc. 94 (1) (1971) 63–67.

[30] D. Raabe, M. Herbig, S. Sandlöbes, Y.J. Li, D. Tytko, M. Kuzmina, P.-P. Choi, Grain boundary segregation engineering in metallic alloys: a pathway to the design of interfaces, Curr. Opin. Solid State Mater. Sci. 18 (4) (2014) 253–261.

[31] D. Raabe, S. Sandlobes, J. Millan, D. Ponge, H. Assadi, M. Herbig, P.P. Choi, Segregation engineering enables nanoscale martensite to austenite phase transformation at grain boundaries: a pathway to ductile martensite, Acta Mater. 61 (16) (2013) 6132–6152. http://dx.doi.org/10.1016/j.actamat.2013.06.055.

[32] E. Rauch, M. Véron, Automated crystal orientation and phase mapping in TEM, Mater. Charact. 98 (2014) 1–9.

[33] E.F. Rauch, J. Portillo, S. Nicolopoulos, D. Bultreys, S. Rouvimov, P. Moeck, Automated nanocrystal orientation and phase mapping in the transmission electron microscope on the basis of precession electron diffraction, Z. Kristallogr. 225 (2–3) (2010) 103–109. http://dx.doi.org/10.1524/zkri.2010.1205.

[34] X. Sauvage, W. Lefebvre, C. Genevois, S. Ohsaki, K. Hono, Complementary use of transmission electron microscopy and atom probe tomography for the investigation of steels nanostructured by severe plastic deformation, Scr. Mater. 60 (12) (2009) 1056–1061. http://dx.doi.org/10.1016/j.scriptamat.2009.02.019.

[35] Y. Toji, H. Matsuda, M. Herbig, P.-P. Choi, D. Raabe, Atomic-scale analysis of carbon partitioning between martensite and austenite by atom probe

tomography and correlative TEM, Acta Mater. 65 (2014) 215–228 10.1016/j.actamat.2013.10.064.
[36] M. Tomozawa, Y. Miyahara, K. Kako, Solute segregation on Sigma 3 and random grain boundaries in type 316L stainless steel, Mater. Sci. Eng. A – Struct. Mater. Prop. Microstruct. Process. 578 (2013) 167–173. http://dx.doi.org/10.1016/j.msea.2013.04.048.
[37] P.W. Trimby, Orientation mapping of nanostructured materials using transmission Kikuchi diffraction in the scanning electron microscope, Ultramicroscopy 120 (2012) 16–24. http://dx.doi.org/10.1016/j.ultramic.2012.06.004.
[38] D.B. Williams, C.B. Carter, Transmission Electron Microscopy, Part 1: Basics, 2nd edition,. Springer Science, Business Media, NY, USA, 2009.
[39] L. Yao, M.P. Moody, J.M. Cairney, D. Haley, A.V. Ceguerra, C. Zhu, S.P. Ringer, Crystallographic structural analysis in atom probe microscopy via 3D Hough transformation, Ultramicroscopy 111 (6) (2011) 458–463. http://dx.doi.org/10.1016/j.ultramic.2010.11.018.
[40] L. Yao, S.P. Ringer, J.M. Cairney, M.K. Miller, The anatomy of grain boundaries: their structure and atomic-level solute distribution, Scr. Mater. 69 (8) (2013) 622–625. http://dx.doi.org/10.1016/j.scriptamat.2013.07.013.
[41] S. Zaefferer, New developments of computer-aided crystallographic analysis in transmission electron microscopy, J. Appl. Crystallogr. *33* (2000) 10–25. http://dx.doi.org/10.1107/S0021889899010894.
[42] S. Zaefferer, A critical review of orientation microscopy in SEM and TEM, Cryst. Res. Technol. 46 (6) (2011) 607–628. http://dx.doi.org/10.1002/crat.201100125.